



Contents lists available at ScienceDirect

International Journal of Solids and Structures

journal homepage: www.elsevier.com/locate/ijsolstr

The blast resistance of sandwich composites with stepwise graded cores

Erheng Wang, Nate Gardner, Arun Shukla*

Dynamic Photomechanics Laboratory, Department of Mechanical Engineering and Applied Mechanics, The University of Rhode Island, Kingston, RI 02881, USA

ARTICLE INFO

Article history:

Received 9 February 2009

Received in revised form 28 May 2009

Available online 9 June 2009

Keywords:

Sandwich structures
Discretely layered core
Shock wave loading
Dynamic failure
High speed imaging

ABSTRACT

Shock tube experiments were performed to study the dynamic response of sandwich panels with E-Glass Vinyl Ester (EVE) composite face sheets and stepwise graded styrene foam cores. Two types of core configurations, with identical areal density, were subjected to the shock wave loading. The core layers were arranged according to the density of the respective foam; configuration 1 consisted of low/middle/high density foams and configuration 2 consisted of middle/low/high density foams. The method to calculate the incident and reflected energies of the shock wave, as well as the deformation energy of the specimen, were proposed based on the shock wave pressure profiles and the high speed deflection images that were obtained. The experimental results showed that configuration 1 outperformed configuration 2 in regards to their blast resistance. Significant core material compression was observed in configuration 1, while in configuration 2 the core layers disintegrated and the front skin (blast side) fractured into two pieces along the midsection. The estimated energies were then calculated for both configurations. The total energy difference between the incident and reflected energies was almost identical, even though the deformation energy for configuration 2 was larger.

© 2009 Elsevier Ltd. All rights reserved.

1. Introduction

Sandwich structures have important applications in the naval and aerospace industry. Their high strength/weight ratio and high stiffness/weight ratio play a vital role in their applications, especially when they are subjected to high-intensity impulse loadings such as air blasts. Their properties assist in dispersing the mechanical impulse that is transmitted into the structure and thus protect anything located behind it (Xue and Hutchinson, 2003; Fleck and Deshpande, 2004; Dharmasena et al., 2008).

The core materials play a crucial role in the dynamic behavior of sandwich structures when they are subjected to blast loading. The general core materials include polymer foams, metal foams, metal honeycomb, balsa wood, and truss structures, etc. In recent years, stepwise graded materials, where the material properties vary gradually or layer-by-layer within the material itself, were utilized as a core material in sandwich composites. Since the properties of graded/layered core structures can be designed and controlled, they show great potential to be an effective core material for absorbing the blast energy and improving the overall blast resistance of sandwich structures.

The behaviors of sandwich composites under blast loading have been widely studied. Fleck and Deshpande (2004) have theoretically studied the dynamic response of sandwich beams under air and underwater blast loading. They divided the structural response

into three sequential steps and then developed performance charts of the sandwich beams with different core materials in order to find an optimal design. Dharmasena et al. (2008), Nurick et al. (2009), and Zhu et al. (2008) have tested sandwich structures with a metallic honeycomb core material. Their results indicated that the parameters of core materials can effectively reduce the damage of the back face sheet. Radford et al. (2006) has conducted metal foam projectile impact experiments to simulate a blast loading on sandwich structures with metal foam cores, and he found that the ability of sandwich panels to resist dynamic loading is far more superior to that of monolithic metal plates with the same areal density. Tekalur et al. (2009) have studied the dynamic behavior of sandwich structures with reinforced polymer foam cores. They concluded that the imparted damage was substantially reduced when Z-direction pin reinforcements were introduced into the core material. Li et al. (2008) proposed a higher order non-linear core theory and incorporated it into the constitutive equations of core materials. They used this model to obtain the transient response of a shallow shell sandwich composite subjected to blast loading. In addition to the previous works, the behaviors of sandwich structures with designable micro structure core materials have been studied under blast loading in recent years (McShane et al., 2006; Wadley et al., 2008).

However, there have been no results, past or present, regarding the dynamic properties of sandwich composites with a stepwise graded core material under blast loading. Only the behaviors of sandwich composites with stepwise graded core under contact loadings, such as low-velocity impact, have been reported, and

* Corresponding author. Tel.: +1 401 874 2283; fax: +1 401 874 2950.
E-mail address: shuklaa@egr.uri.edu (A. Shukla).

even these reports are limited. The numerical investigation by Apetre et al. (2006) has shown that a reasonable core design can effectively reduce the shear forces and strains within the structures. Consequently, they can mitigate or completely prevent impact damage on sandwich composites. Li et al. (2001) examined the impact response of layered and graded metal-ceramic structures numerically. He found that the choice of gradation has a great significance on the impact applications and the particular design can exhibit better energy dissipation properties.

The present study focuses on the blast resistance and energy absorption of sandwich composites with a stepwise graded foam core when experimentally subjected to a shock wave loading. The results will help to understand the performance and the mechanisms of failure of sandwich composites with a stepwise graded core under blast loading and provide a guideline for a better core design. The quasi-static and dynamic constitutive behaviors of the foam core materials were first studied using a modified SHPB device with a hollow transmitter bar. The sandwich composites with two types of layered foam core arrangements were then fabricated and subjected to shock wave loading generated by a shock tube. The two types of sandwich composites have identical core materials but different core layer arrangements. The shock pressure profiles and real time deflection images were carefully analyzed to reveal the failure mechanisms of these sandwich composites.

Based on the experimental data, the methods to calculate the energies of the incident shock wave (incident energy), the reflected shock wave (reflected energy), and the energy that deforms the specimen (deformation energy) were proposed and implemented. The energy redistribution in the system was analyzed, and the results showed that only a small amount of incident energy of the shock wave was transferred into the sandwich composites during the shock wave loading process.

2. Energy evaluation

The incident energy, the reflected energy, and the deformation energy were calculated based on the shock wave pressure profiles and the high speed deflection images obtained from the shock tube experiment. Fig. 1 shows a shock wave loading process with a shock tube. The definite state of the gas can be defined using the following physical parameters:

- p the pressure
- ρ the gas density
- u the gas particle speed
- c the speed of sound in gas

The subscript 0 on the parameters denotes the initial state of the gas. Subscript 1 represents the state of the gas located behind the incident shock wave front and it will be defined as the incident state. Subscript 2 represents the state of the gas located behind the reflected shock wave front and it will be defined as the reflected state.

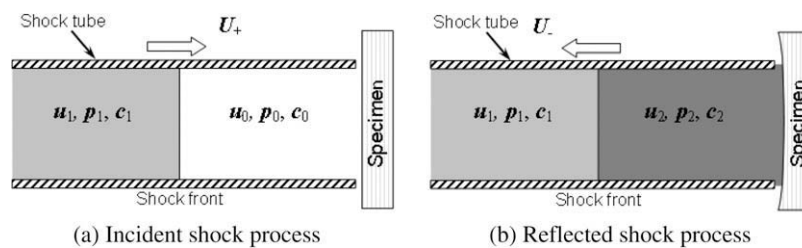


Fig. 1. Sketch of the incident and the reflected shock process.

2.1. The incident and reflected energies

The calculation of the incident and reflected energies is based on the incident and reflected shock wave pressure profiles. When a planar shock wave impacts a planar panel, the energy stored in the gas, which is located behind the shock wave front, will impinge on the structure. The stored energy in the gas is equivalent to the work done by the gas as it propagates through the cross-section of the shock tube. Note that the particle speed, u , of the gas located behind the shock wave front is important in evaluating the energies, and it is always less than the propagating speed, U , of the wave front. When a shock wave with a pressure profile, $p(t)$, propagates within a shock tube with a cross-sectional area, S , it induces a particle speed, u and impacts a specimen, then the energy stored in the impinging gas during element time, dt , is equivalent to $p(t)S u dt$. Therefore, the total energy can be obtained by integrating $p(t)S u dt$ with respect to time. The formulas for $E_{incident}$ and $E_{reflected}$ are as follows:

$$E_{incident} = \int [p_1(t) S u_1] dt \tag{1}$$

$$E_{reflected} = \int [p_2(t) S u_2] dt \tag{2}$$

where $p_1(t)$ is the incident pressure profile, u_1 is the particle speed behind the incident shock front, $p_2(t)$ is the reflected pressure profile, and u_2 is the particle speed behind the reflected shock front. The incident energy, $E_{incident}$, is the energy stored in the gas located behind the incident shock wave front, while the reflected energy, $E_{reflected}$, is the energy stored in the gas located behind the reflected shock wave front, respectively.

In Eqs. (1) and (2), the cross-sectional area, S , of the shock tube is known and the incident and reflected pressure profiles, $p_1(t)$ and $p_2(t)$, can be measured. The particle speeds, u_1 and u_2 behind the incident and reflected shock front can be calculated using the theory of gas dynamics (Courant and Friedrichs, 1948).

Based on the Hugoniot relation of the polytropic gas and the jump conditions for the shock wave, we can derive the following equations (using incident shock process in Fig. 1a as an example):

$$\frac{p_1}{p_0} = (1 + \mu^2) M_0^2 - \mu^2 \tag{3a}$$

$$\text{or } \frac{p_0}{p_1} = (1 + \mu^2) M_1^2 - \mu^2 \tag{3b}$$

and

$$(1 - \mu^2)(U_+ - u_0)^2 - (u_1 - u_0)(U_+ - u_0) = (1 - \mu^2)c_0^2 \tag{4a}$$

$$\text{or } (1 - \mu^2)(U_+ - u_1)^2 - (u_0 - u_1)(U_+ - u_1) = (1 - \mu^2)c_1^2 \tag{4b}$$

where $\mu^2 = \frac{\gamma-1}{\gamma+1}$, γ is the adiabatic exponent of the gas, M is the Mach number, $M_1 = \frac{u_1 - u_+}{c_1}$ and $M_0 = \frac{u_0 - u_+}{c_0}$, U_+ and U_- are the incident and reflected shock front speeds, velocities, respectively. p_0 and p_1 are the pressures at different locations.

In the present experiments, the incident and reflected processes (as shown in Fig. 1a and b) generate a system of four independent equations and they are defined by Eqs. (3) and (4). There are 12

parameters in these equations namely: $p_0, p_1, p_2, u_0, u_1, u_2, c_0, c_1, c_2, U_+, U_-$, and γ . Note u_0 is zero, c_0 is 340 m/s (speed of sound in air), the adiabatic exponent, γ , is a gas constant and p_0, p_1, p_2, U_+, U_- can be measured. Therefore, there exist only four unknown parameters, u_1, u_2, c_1 , and c_2 . The particle speeds behind the shock wave can be solved explicitly as Eq. (5).

$$u_1 = \frac{(1 - \mu^2)(U_+^2 - c_0^2)}{U_+} \tag{5a}$$

$$u_2 = \frac{(1 - \mu^2)(U_+^2 - c_0^2)}{U_+} + (1 - \mu^2) \left[\frac{(1 - \mu^2)(U_+^2 - c_0^2)}{U_+} + U_- \right] \left[\frac{(1 + \mu^2)}{(p_2/p_1) + \mu^2} - 1 \right] \tag{5b}$$

By assuming these particle speeds to be constant during the shock wave loading process, the incident and reflected energies can then be calculated by substituting Eq. (5) into Eqs. (1) and (2).

2.2. The deformation energy

The calculation of the deformation energy is based on the reflected shock wave pressure profile and the high speed deflection images. The main idea is to obtain the deflection–time data from the high speed deflection images and the force–time data from the reflected pressure profile. Combining the deflection–time data and the force–time data will result in force–deflection data. Then the deformation energy can be obtained by integrating the force–deflection data.

The measurement of the deflection is the most important step in this energy calculation. Since the force is only applied on the front face of the specimen, the deflection of the front face of the specimen is what we need. As shown in Fig. 2a, seven points were chosen along the profile of the front face of the specimen in the high speed images, and a spline curve fitting was applied to match the shape of the front face. After calibrating the distance and choosing the reference point, we can calculate the deflection of every point on the front face. Thus, the deflection–time data can be obtained. Fig. 2b shows the typical deflection–time data obtained from this process. By assuming that the pressure applied on the shock area is uniform and combining the pressure–time data and the deflection–time data, the pressure–deflection profile can be obtained, as shown in Fig. 2c. Therefore, the deformation energy ($E_{deformation}$) can be calculated by integrating the pressure–deflection profile of every point inside the shock area. The formula is as follows:

$$E_{deformation} = \oint_{S_{tube}} \left(\int p_2(t) dl_{deflection} \right) dS \tag{6}$$

3. Material and specimen

3.1. Skin and core materials

The skin materials that were utilized in this study were E-Glass Vinyl Ester (EVE) composites. The woven roving E-glass fibers of the skin material were placed in a quasi-isotropic layout [0/45/90/−45]_s. The fibers were made of the 18 oz/yd² area density plain weave. The resin system used was Ashland Derakane Momentum 8084 and the front skin and the back skin consisted of identical layout and materials.

The core materials used in the present study were Corecell™ A series styrene foams, which were manufactured by Gurit SP Technologies specifically for marine sandwich composite applications. The three types of Corecell™ A foam that were used in the present study were A300, A500, and A800. Table 1 listed important material properties of the three foams from the manufacturer’s data (<http://www.gurit.com>).

The cell structures for the three foams were very similar and the only difference appears in the cell wall thickness and node sizes, which accounted for the different densities of the foams.

3.2. Sandwich panels with graded core

The VARTM-fabricated panels were produced from a plain weave E-glass fabric type. Fabric lay-up was an 8-ply balanced/symmetric quasi-isotropic layout [0/45/90/−45]_s. For the core, each layer of foam was 12.7 mm thick. The overall dimensions for the samples were 102 mm wide, 254 mm long, and 48 mm thick. The foam core itself was 38 mm thick, while the skin thickness was 5 mm. The average areal density of the samples was 19.02 kg/m².

Two types of sandwich specimens with different core layer gradation were studied (as shown in Fig. 3a). Configuration 1 consisted of a core gradation of A300/A500/A800 (low/middle/high density), and configuration 2 consisted of a core gradation of A500/A300/A800 (middle/low/high density). With these configurations it should be noted that the first core layer was the one first subjected to the shock wave loading. An actual sample can be seen in Fig. 3b.

Table 1 Material properties for foam core (<http://www.gurit.com>).

	Nominal density (kg/m ³)	Compressive modulus (MPa)	Shear elongation (%)
A300	58.5	32	62
A500	92	64	69
A800	150	117	50

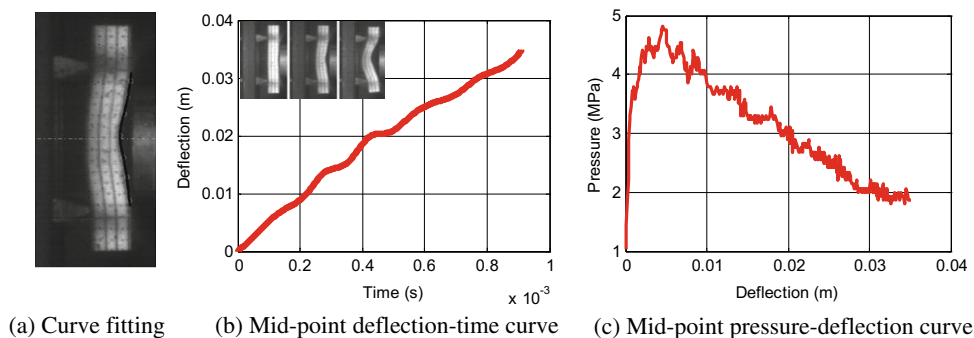


Fig. 2. Deflection based on high speed images and pressure profile.

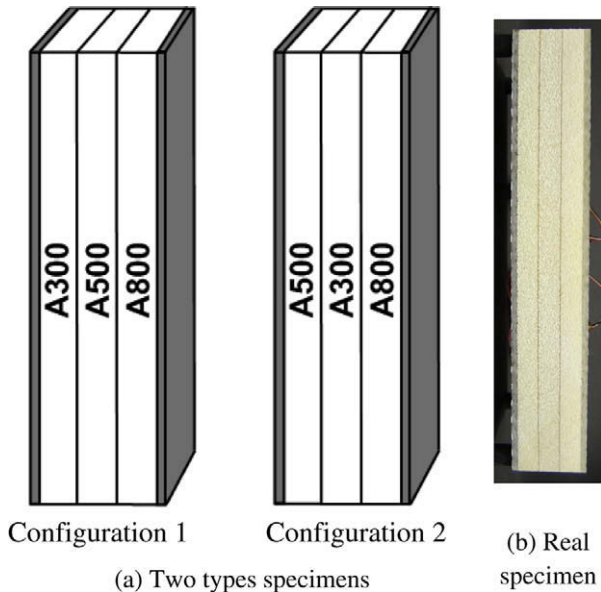


Fig. 3. Specimen configuration.

4. Experimental setup and procedure

4.1. Modified split Hopkinson pressure bar with hollow transmitter bar

Split Hopkinson Pressure Bar (SHPB) is the most common device for measuring dynamic constitutive properties of materials. Due to the low-impedance of Corecell™ foam materials, dynamic experiments for the core materials were performed with a modified SHPB device with a hollow transmitter bar to increase the transmitted signal intensity. A sketch of the modified SHPB device and typical pulse profiles were given in Fig. 4. It had a 304.8 mm-long striker, 1600 mm-long incident bar and 1447 mm-long transmitter bar. All of the bars were made of a 6061 aluminum alloy. The nominal outer diameters of the solid incident bar and hollow transmitter bar were 19.05 mm. The hollow transmitter bar had a 16.51 mm inner diameter. At the head and at the end of the hollow transmitter bar, end caps made of the same material as the bar were pressure fitted into the hollow tube. By applying pulse shapers, the effect of these end caps on the stress waves can be minimized. The details of the analysis and derivation of equations for analysis of experimental data can be found in Chen's paper (1998).

4.2. Shock tube

A shock tube apparatus was utilized to obtain the controlled blast loading (Fig. 5a). It had an overall length of 8 m, consisting

of a driver, driven and muzzle section. The high-pressure driver section and the low pressure driven section were separated by a diaphragm. By pressurizing the high-pressure section, a pressure difference across the diaphragm was created. When this difference reached a critical value, the diaphragms ruptured. This rapid release of gas created a shock wave, which travelled down the tube to impart dynamic loading on the specimen.

Fig. 5b showed detailed dimensions and locations of the muzzle, specimen, supports and the pressure sensors (PCB102A). The sensors were mounted at the end of the muzzle section to measure the pressure profiles during the experiment. The final muzzle diameter was 0.0762 m. The distance between the two sensors was 0.16 m and the distance between the second sensor and the end of the muzzle was ~ 0.02 m. The specimen was placed in the support fixture, which ensured simply supported boundary conditions with a 0.1524 m span. The front face of the specimen was normal to the axis of the shock tube and had a ~ 1.6 mm initial gap to the muzzle end.

4.3. Experimental procedure and parameters

In the present study, a simply stacked diaphragm of 5 plies of 10 mil mylar sheets with a total thickness of 1.27 mm was utilized to generate an impulse loading on the specimen with an incident peak pressure of approximately 1 MPa and a wave speed of approximately 1030 m/s. For each configuration, at least three samples were tested. A high speed digital camera, IMACON 200, was used to capture the real time side-view deformation of the specimen. With an inter-frame time of 70 μ s and an exposure time of 700 ns, approximately 14 frames could be obtained. Fig. 6 showed the experimental setup.

Fig. 7a showed the pressure profile associated with the incident pulse in the absence of a target. This pressure profile was used in calculating the total incident energy. Fig. 7b showed the reflected pressure profile obtained by the transducer located at the muzzle end and this pressure profile was used in the calculation of reflected energy as well as the deformation energy of the specimen.

5. Experimental results and discussion

5.1. Dynamic behavior of core material

The three types of Corecell™ A foams have different quasi-static and dynamic behaviors. For the same type of Corecell™ A foam, the material behavior under high strain rate loading is significantly different from its behavior under quasi-static loading.

Fig. 8 showed the quasi-static and high strain-rate behavior of the different types of Corecell™ A foams. For quasi-static behavior, the stress–strain curves showed three deformation regions. The first one was the elastic region; the second was the plateau stress

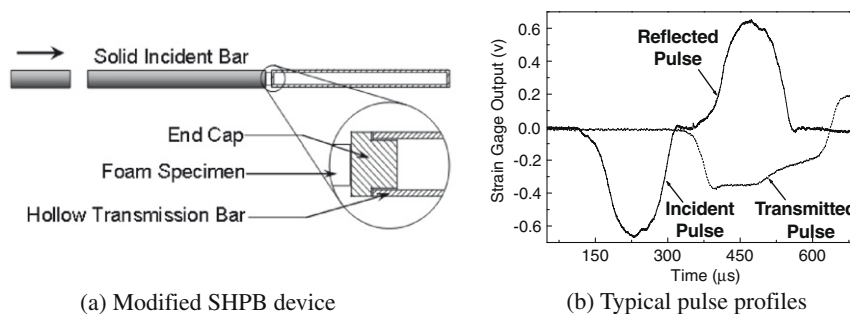


Fig. 4. Sketch of modified SHPB device with hollow transmitter bar and typical pulse profiles.

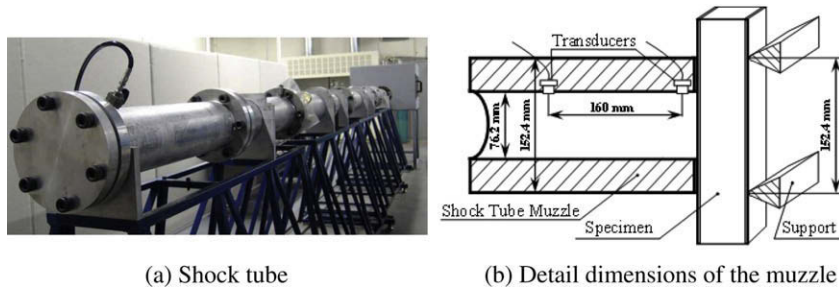


Fig. 5. Shock tube apparatus.

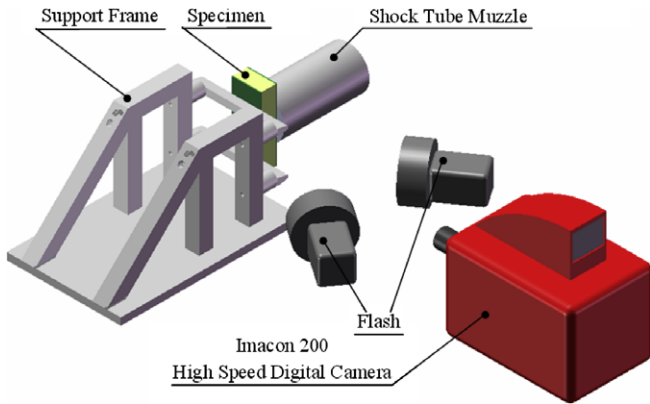


Fig. 6. Experimental setup.

region and the third was the densification region. For high strain-rate behavior, the stress–strain curves also showed elastic and plateau stress regions though the strain did not reach the densification region. The plateau stress regions for both instances had a large strain range. This showed the high energy absorption ability of these foams under low stress levels.

As seen in Fig. 8, the quasi-static and dynamic stress–strain responses had an obvious trend for the different types of foams. Lower density foam has a lower strength and stiffness, as well as a larger strain range for the plateau stress.

The high strain-rate yield stresses and plateau stresses were much higher than the quasi-static ones for the same type of foam. Table 2 showed the quasi-static and high strain-rate yield stresses. The dynamic strength of A500 and A800 increased approximately 100% in comparison to their quasi-static strength, while A300 increased approximately 50%. The high yield stresses and long stress plateaus indicated that these foams can bear higher stresses and absorb larger amounts of energy. Therefore, they showed great potential in being used as core materials in sandwich structures subjected to high intensity blast loading.

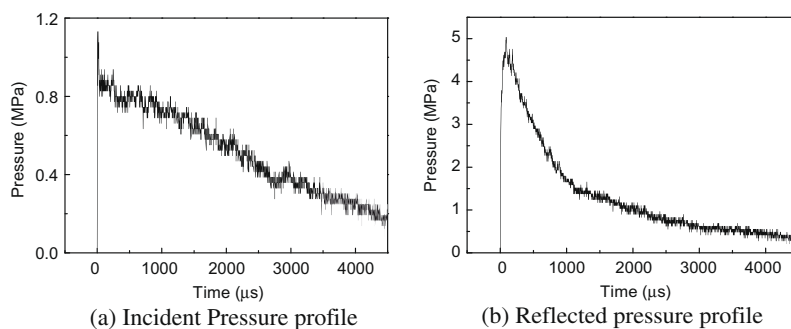


Fig. 7. Shock wave pressure profiles.

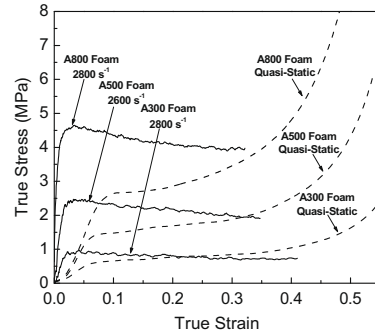


Fig. 8. Quasi-static and high strain-rate behaviors of different types of Corecell™ A foams.

5.2. Response of sandwich composites with graded cores

5.2.1. Real time deformation

The real time observations of the transient behavior of configuration 1 (A300/A500/A800) and configuration 2 (A500/A300/A800) under shock wave loading were shown in Figs. 9 and 10, respectively. The shock wave propagated from the right side of the image to the left side and some detailed deformation mechanisms were pointed out in the figures.

For configuration 1, as shown in Fig. 9, the first core layer subjected to the shock wave was A300 and the core gradation was from the foam of least density and lowest strength to the foam of highest density and highest strength.

In this case, two deformation mechanisms were observed during the panel deflection: core compression and global bending. The indentation failure of the front skin can be observed at $t = 70 \mu\text{s}$. Core compression of the A300 foam, the first core layer of gradation, can initially be observed at $140 \mu\text{s}$. At this time there is no compression in the other two core layers of foam. Due to the compression of the foam, the high dynamic pressure applied

Table 2
Yield strength of Corecell™ A foams.

Foam type	A300	A500	A800
Quasi-static yield stresses (MPa)	0.60	1.35	2.46
High strain-rate yield stresses (MPa)	0.91	2.47	4.62

to the front skin was substantially weakened by the time it reached the back skin. The measurements showed that at $t = 420 \mu\text{s}$ and onward the central deflection of the A300 foam was approximately 25% more than that of the A500 and A800 foams. This deflection can be directly related to the density of the A300 foam and its compressive strength. The double-winged deformation shape showed that the core of the sandwich structure was under intense shear loading. The onset of core failure, where core cracking begins, was observed at $t = 280 \mu\text{s}$ and the initial separation/delamination of the front skin from the core was observed at $t = 770 \mu\text{s}$; this indicated relatively weak adhesion. Even though the onset of core failure began at $t = 280 \mu\text{s}$, complete core collapse and failure was not observed in this configuration.

In configuration 2, as shown in Fig. 10, A500 was the first core layer subjected to the shock wave and the core gradation began with the foam of middle density and middle strength, next the

foam of least density and lowest strength, and then the highest density and highest strength foam.

In this case, the only deformation mechanism observed was global bending. The images in Fig. 10 showed that indentation failure of the front skin began at $t = 70 \mu\text{s}$. Also note that the central core compression was not as prominent in this sandwich as can be seen in configuration 1. The initial separation/delamination of the core began at $t = 350 \mu\text{s}$ and was located between the A500 and A300 foams. The onset of core failure, where core cracking began, can be seen at $t = 140 \mu\text{s}$ and the onset of complete collapse of the core initiates at $t = 490 \mu\text{s}$, where the core cracking had traveled completely through the core.

The major failure mechanism in configuration 2 was progressive damage of the core and the sandwich, which initiated at the back skin and was evident in Fig. 10. This crack became a large inclined crack and propagated through the core from the back skin to the front skin. By $t = 490 \mu\text{s}$ the crack had extended completely through the core and delamination between the A300 and A500 foam was very prominent. Also at this time, many cracks were visible in the core which is followed by a rapid crushing of the core and catastrophic failure of the sandwich structure. This showed that configuration 2 cannot withstand the applied shock wave pressure, which had a peak value of $\sim 4.83 \text{ MPa}$.

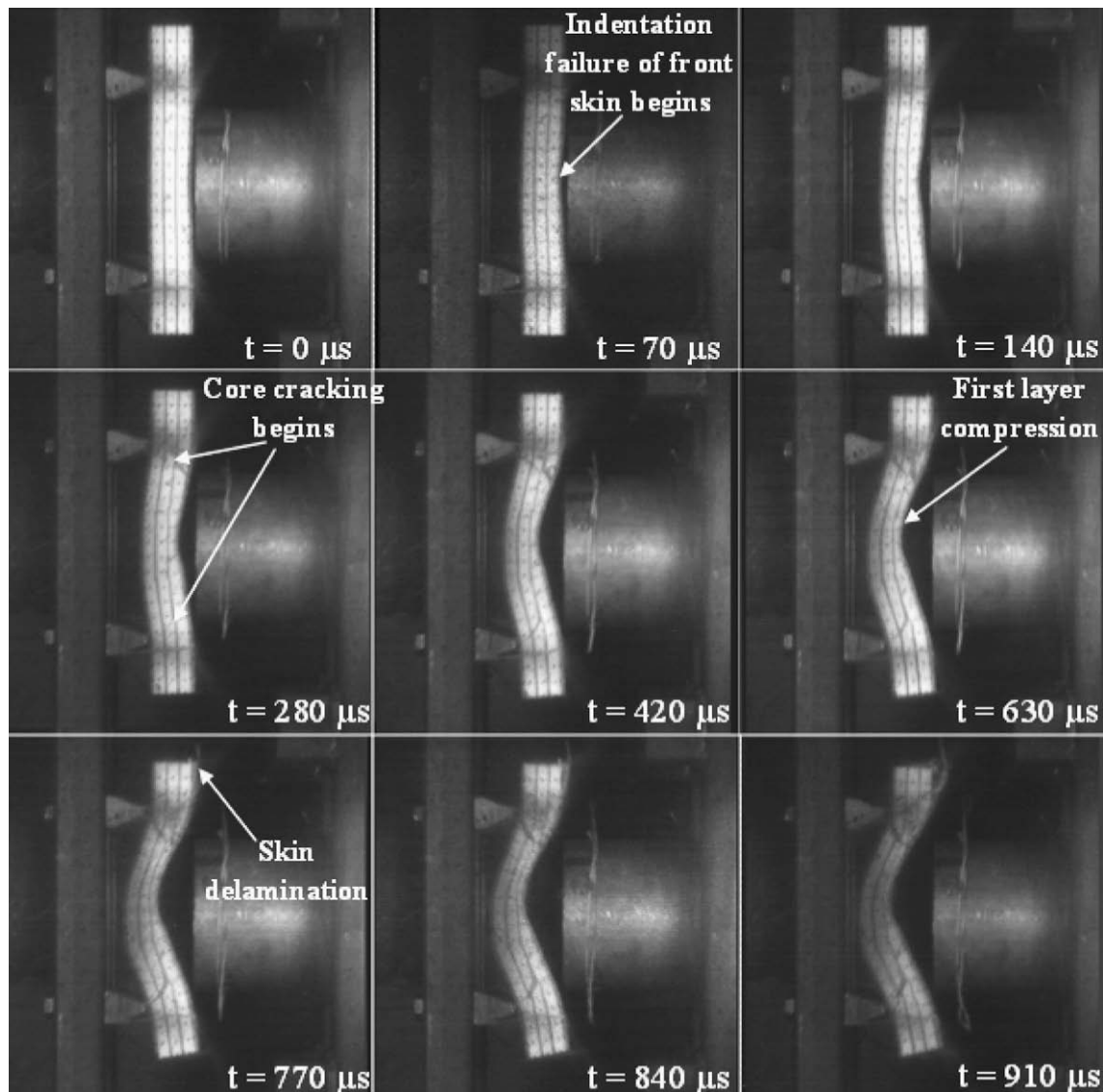


Fig. 9. Real time side view images of configuration 1 (A300/A500/A800) under shock loading.

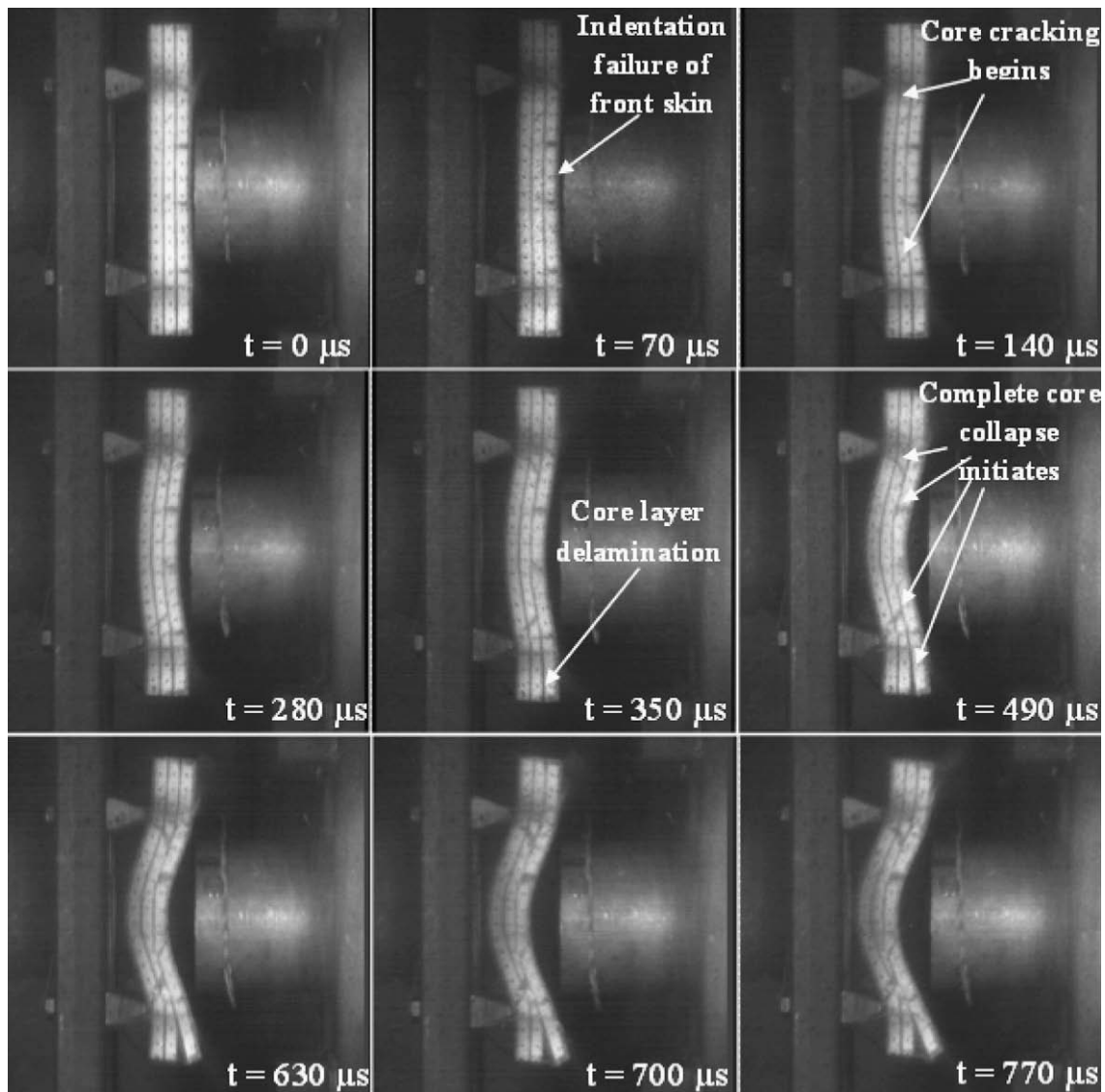


Fig. 10. Real time side view images of configuration 2 (A500/A300/A800) under shock loading.

Contrary to the case of configuration 2 the real time deformation sequences observed in Fig. 9 for configuration 1 indicated that the major failure mechanism was core compression. The results showed that the core lay-up improved the overall performance of the structure. The onset of core failure took twice as long to be visible in this configuration as opposed to configuration 2 and no complete core collapse was evident. Even though delamination did occur, it was between the face sheet and foam core only. Overall configuration 1 outperformed configuration 2, and this was related to the dynamic constitutive behaviors of the foam core materials and the order of the core layer arrangements. For configuration 1, the strength of the core layers increase monotonously from the front face sheet to the back face sheet. Due to the low yield stress of the first core layer, A300, under dynamic loading, core compression occurred before the sandwich panel exhibited any bending (indentation failure in Fig. 9) and the core layers were compressed layer by layer. For configuration 2, the strength of the core layers did not increase monotonously from the front face sheet to the back face sheet. Here the first core layer, A500, had higher strength in comparison to A300 foam. These factors neutralized the core compression even though the core materials were

identical. Thus bending occurred before the sandwich panel exhibited core compression.

5.2.2. Deflection

The mid-point deflections of each graded sandwich panel and all of its constituents were obtained from the high speed images. The deflection of the front face (front skin), interface 1 (between first and second core layer), interface 2 (between second and third core layer), and back face (back skin) for configuration 1 and configuration 2 were plotted in Figs. 11 and 12. It can be seen in Fig. 11 for configuration 1 that the front face deflects to ~ 33 mm at $\sim t = 840$ μ s, which was approximately 25% more than the other three constituents. Note that the difference between the front face (skin) and interface 1 was the A300 foam, which was the weakest foam in three types of foams, and almost all compression occurs here (~ 7 mm).

On the contrary, all of the constituents of configuration 2 deflect in the same manner (shown in Fig. 12). This showed almost no obvious compression, even though the core foams of configuration 1 and configuration 2 were identical, but in a different gradation. Also this graded sandwich panel only deflected to ~ 29 mm at $\sim t = 840$ μ s.

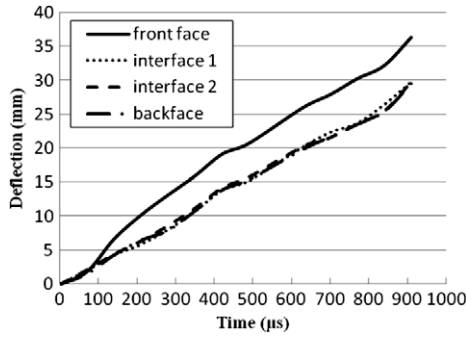


Fig. 11. Deflection of A300/A500/A800.

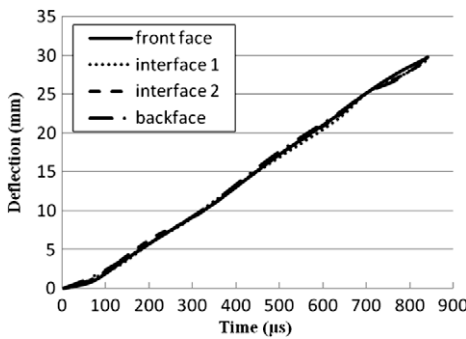


Fig. 12. Deflection of A500/A300/A800.

5.2.3. Post-mortem analysis

The damage patterns in the graded sandwich composites after the shock event occurred were visually examined and recorded using a high resolution digital camera and were shown in Fig. 13.

When configuration 1 was subjected to the highly transient loading, the damage was confined to the area where the supports were located in the shock tube and core cracking was visible in these two areas. Delamination was visible between the front skin and the foam core, as well as the back skin and the foam core. The core compression can be seen clearly and distinctively in the A300 foam.

Microscopic analysis of the failure and compression observed in configuration 1 was done using a Nikon SMZ microscope. Pre and post-blast core cell structures for the three layers of gradation were shown in Fig. 14. Note the heavy amount of compression seen in the A300 foam core cell structure. Also the cell structure for the A500 foam did indeed compress, but not nearly as much as can be seen in the A300 foam. Likewise, the A800 foam core cell structure did compress, but only minimally.

Unlike the damage visible in configuration 1, configuration 2 suffered catastrophic damage as shown in Fig. 13. The core of the sandwich disintegrated and the front skin (blast side) of the sandwich fractured into two pieces at the midsection. The back skin showed an extensive amount of fiber delamination in the central region as well.

Fig. 15 showed the details of the failure mode in configuration 2. The photograph showed a flat segment located at the incident face indicating that the stresses were released in this region. The cracks observed on both sides of the flat segment do not resemble those caused by the bending shear stresses which were typical near the supports. The detailed macroscopic images of the local cracks and delamination surfaces showed that the delamination surfaces exhibit similar material granules as those observed in a pure tension test.

5.2.4. Energy evaluation

The energies calculated by the methods described in Section 2 were shown in Figs. 16 and 17. With regards to the choice of the adiabatic component, γ , the following explanation was offered. In the present shock tube experiments, prior to the diaphragm rupturing, one side of the diaphragm was helium (driver side), while the other side of the diaphragm was air (driven side). After the diaphragm ruptured the compressive shock wave travelled in the direction of higher pressure to lower pressure (helium \rightarrow air). Since the particle speed of the gas (helium) located behind the shock front was less than the speed of the shock front itself, air passed over the shock front and occupied the space located between the gas (helium) and the shock front during the propagation of the shock wave. Therefore, by the time the shock wave reached the specimen, the gas located to the front and back side of the shock front were both airs. Thus, the adiabatic exponent of air, $\gamma = 1.4$, was used in the energy calculations.

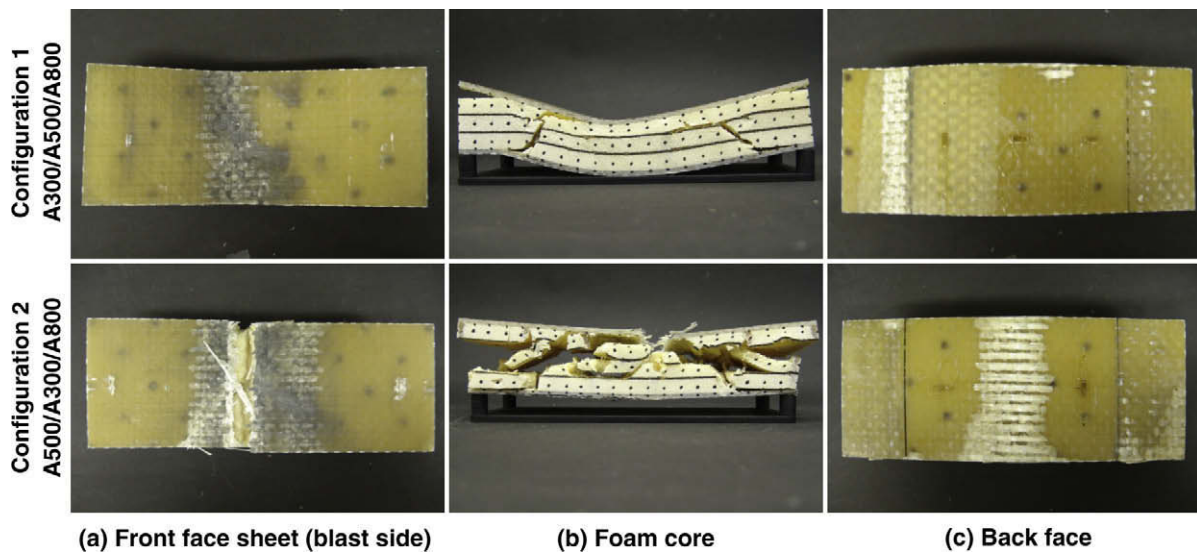


Fig. 13. Visual examination of sandwich composites after being subjected to high intensity blast load.

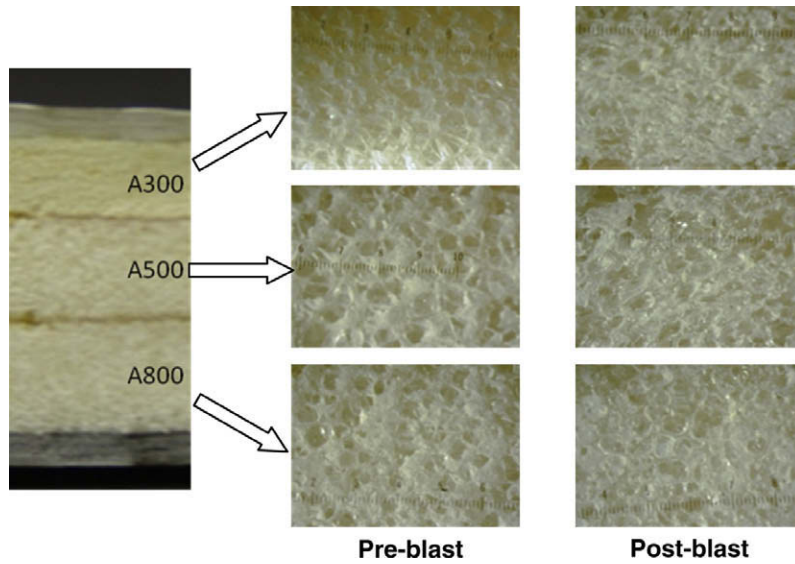


Fig. 14. The failure and compression of core foam cell microstructure in configuration 1.

Fig. 16 showed the incident and reflected energy calculated for configuration 1 (A300/500/800). The difference between the incident and reflected energies was the total energy lost during the shock wave loading process. It included the energy absorbed by the composite structures, sound, light, heat, rigid body motion, and other forms of energy. We defined it as the total amount of energy loss. It can be seen that there is a large amount of energy lost during the shock wave loading process.

The initial gap between the specimen and the muzzle end (~1.6 mm) increased after the impingement of shock on the specimen as the specimen deformed in a concave manner. The gas leak from this gap did affect the reflected energy calculation as it influenced the reflected pressure drop. Therefore a fraction of energy was lost due to the gas that escaped from this gap. This lost energy was included in our estimation of the total energy loss.

Fig. 17a compared the total energy loss of configuration 1 (A300/500 /800) and configuration 2 (A500/300/800), while Fig. 17b compared the deformation energy of configuration 1 and configuration 2, respectively. It can be seen in Fig. 17a that the total

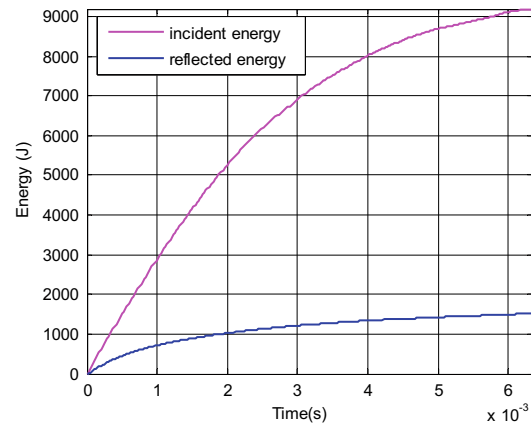


Fig. 16. Incident and reflected energies of configuration 1 (A300/A500/A800).

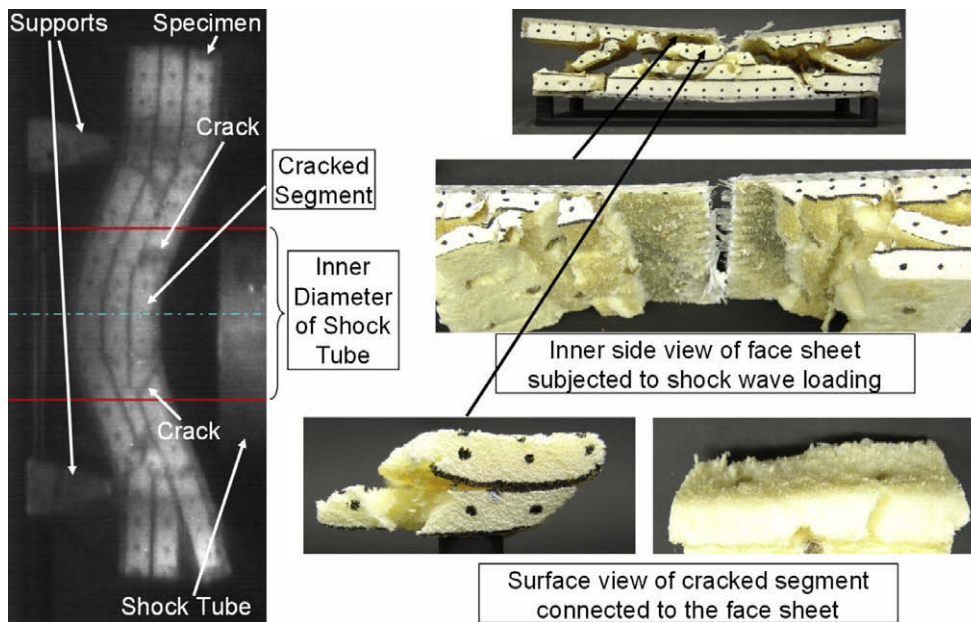


Fig. 15. The details of the failure mode in configuration 2.

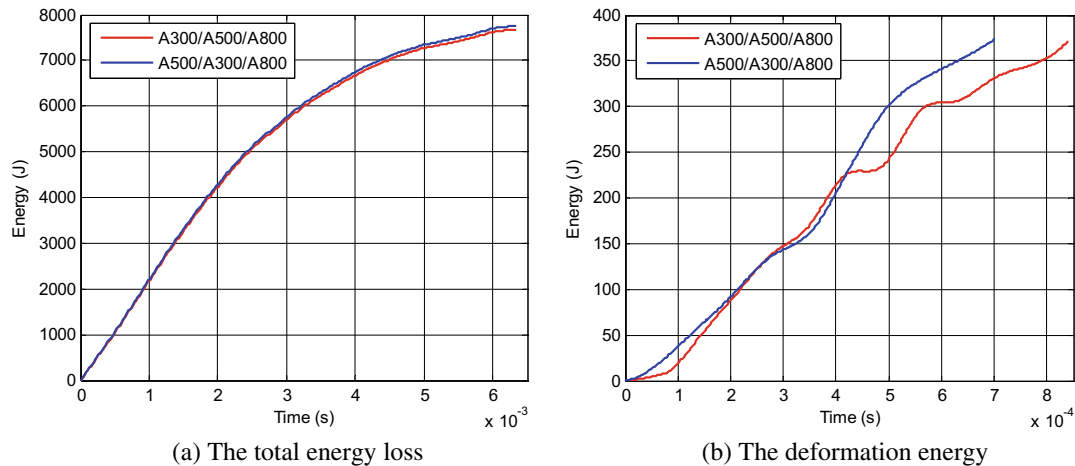


Fig. 17. A comparison of the total energy loss and a comparison of the deformation energy for two configurations.

energy loss for both configurations was almost identical. The deformation energy of configuration 2 (A500/300/800) was a slightly higher than that of configuration 1 (A300/500/800). This minimal difference can be ignored due to the error that arose when measuring the positions and deflection using the high speed images. With that said, these two configuration exhibited similar energy transferring properties when subjected to the same input shock wave loading. Configuration 1 (A300/500/800) showed no obvious structural collapse while configuration 2 (A500/300/800) exhibited total structural collapse. Therefore it can be concluded that configuration 1 (A300/500/800) can withstand a higher blast loading than configuration 2 (A500/300/800) and thus overall outperformed configuration 2.

Due to the fact that the deformation energy (Fig. 17b) was much less than the total amount of energy loss (Fig. 17a), it can be concluded that only a small amount of energy was transferred into the sandwich structure. At 0.6 ms, the total energy loss was approximately 1300 J, while the deformation energy was only ~ 350 J. This indicated that only $\sim 25\%$ of the total energy lost was transferred into the specimen and most of the energy actually dissipated into other forms of energy (sound, heat, light, rigid body motion, and various other forms).

6. Conclusions

- (1) The dynamic stress–strain response was significantly higher than the quasi-static response for every type of Corecell™ A foam studied. Both quasi-static and dynamic constitutive behaviors of Corecell™ A series foams (A300, A500, and A800) showed an increasing trend.
- (2) The sandwich specimens with two different core arrangements, configuration 1 (A300/A500/A800) and configuration 2 (A500/A300/A800), were subjected to shock wave loading. The overall performance of configuration 1 (A300/A500/A800) was better than that of configuration 2 (A500/A300/A800). Large compression was visible in the core when the least density foam (A300) is first in contact with the blast loading. This configuration reduced the dynamic pressures seen on the back face sheet, and thus limited the total amount of damage imparted on the specimen. When using the A500 foam first in contact with the blast loading, the overall deformation process of the sample was completely different. Compression in the core was limited, and thus the specimen showed a heavy amount of damage.
- (3) The methods used to calculate the energy of the incident energy, the reflected energy and the deformation energy

were proposed and implemented. The difference between the total incident and reflected energy was defined as the total energy loss in the system during the shock loading process. Only a small amount of energy was transferred into the specimens during the shock loading process. The total energy loss in the two configurations as well as their deformation energy was almost identical. Therefore, since configuration 2 (A500/A300/A800) showed heavy damage and failure, it can be concluded that overall configuration 1 (A300/A500/A800) outperformed configuration 2 (A500/A300/A800).

Acknowledgement

The authors acknowledge the financial support provided by Dr. Yapa D.S. Rajapakse, under Office of Naval Research (ONR) Grant No. N00014-04-1-0268. The authors acknowledge the support provided by the Department of Homeland Security (DHS) under Cooperative Agreement No. 2008-ST-061-ED0002. Authors also thank Dr. Stephen Nolet and TPI Composites for providing the facility for creating the materials used in this study.

References

- Apetre, N.A., Sankar, B.V., Ambur, D.R., 2006. Low-velocity impact response of sandwich beams with functionally graded core. *International Journal of Solids and Structures* 43 (9), 2479–2496.
- Chen, W., Zhang, B., Forrestal, M.J., 1998. A split Hopkinson bar technique for low-impedance materials. *Experimental Mechanics* 39 (2), 81–85.
- Courant, R., Friedrichs, K.O., 1948. *Supersonic Flow and Shock Waves*. Interscience, New York.
- Dharmasena, K.P., Wadley, H.N.G., Xue, Z., Hutchinson, J.W., 2008. Mechanical response of metallic honeycomb sandwich panel structures to high-intensity dynamic loading. *International Journal of Impact Engineering* 35 (9), 1063–1074.
- Fleck, N.A., Deshpande, V.S., 2004. The resistance of clamped sandwich beams to shock loading. *Journal of Applied Mechanics* 71, 386–401. Available from: <<http://www.gurit.com/>>.
- Li, R.F., Kardomateas, G.A., Simitse, G.J., 2008. Nonlinear response of a shallow: sandwich shell with compressible core to blast loading. *Journal of Applied Mechanics – Transactions of the ASME* 75 (6), 125–138.
- Li, Y., Ramesh, K.T., Chin, E.S.C., 2001. Dynamic characterization of layered and graded sandwich structures under impulsive loading. *International Journal of Solids and Structures* 38 (34–35), 6045–6061.
- McShane, G.J., Radford, D.D., Deshpande, V.S., Fleck, N.A., 2006. The response of clamped sandwich plates with lattice cores subjected to shock loading. *European Journal of Mechanics – A: Solids* 25, 215–229.
- Nurick, G.N., Langdon, G.S., Chi, Y., Jacob, N., 2009. Behavior of sandwich panels subjected to intense air blast: part 1 – Experiments. *Composite Structures*, in press, doi:10.1016/j.compstruct.2009.04.009.
- Radford, D.D., McShane, G.J., Deshpande, V.S., Fleck, N.A., 2006. The response of clamped sandwich plates with metallic foam cores to simulated blast loading. *International Journal of Solids and Structures* 44, 6101–6123.

- Tekalur, S.A., Bogdanovich, A.E., Shukla, A., 2009. Shock loading response of sandwich panels with 3-D woven E-glass composite skins and stitched foam core. *Composite Science and Technology* 69 (6), 736–753.
- Wadley, H.N.G., Dharmasena, K.P., Chen, Y., Dudt, P., Knight, D., Charette, R., Kiddy, K., 2008. Compressive response of multilayered pyramidal lattices during underwater shock loading. *International Journal of Impact Engineering* 35 (9), 1102–1114.
- Xue, Z., Hutchinson, J.W., 2003. Preliminary assessment of sandwich plates subject to blast loads. *International Journal of Mechanical Sciences* 45, 687–705.
- Zhu, F., Zhao, L., Lu, G., Wang, Z., 2008. Deformation and failure of blast loaded metallic sandwich panels – experimental investigations. *International Journal of Impact Engineering* 35 (8), 937–951.